Decrease in magnetosheath jet production due to conditions within Coronal Mass Ejections

Florian Koller[1], Ferdinand Plaschke[2], Manuela Temmer[1], Luis Preisser[3], O. W. Roberts[3], Stefan Weiss[1], Zoltan Vörös[3,4]

[1]Institute of Physics, University of Graz, Universitätsplatz 5, 8010 Graz, Austria
[2]Institut für Geophysik und extraterrestrische Physik, TU Braunschweig, Mendelssohnstraße 3, 38106 Braunschweig, Germany
[3]Space Research Institute, Austrian Academy of Sciences, Schmiedlstrasse 6, 8042 Graz, Austria
[4]Institute of Earth Physics and Space Science, ELRN, Csatkai E. u. 6-8, 9400 Sopron, Hungary

Key Points:

- The low number of jets observed during CMEs come from high cone angles and low Alfvén Mach numbers related to the magnetic ejecta.
- We show how both parameters are distributed during times of jet observation compared to reference solar wind times.
- The condition found in CMEs regarding cone angle and Mach number are unfavorable for jet production, hence CMEs decrease the jet occurrence.

Corresponding author: Florian Koller, florian.koller@uni-graz.at

Abstract

Magnetosheath jets are dynamic pressure enhancements observed in the terrestrial magnetosheath. Their generation mechanisms are currently debated but can be linked to foreshock processes. Recent results showed that jets are less numerous when coronal mass ejections (CME) cross the magnetosheath. Here, we show for the first time how CMEs and their magnetic ejecta (ME) region are related to jet production. Based on THEMIS and OMNI data covering 2008–2021, we show the probability distribution of jet production in 2D parameter histograms using the IMF cone angle and Alfvén Mach number. We compare this distribution with the values within CME-MEs. We find high cone angles and low Alfvén Mach numbers within CME-MEs, which both are unfavorable for jet production as they may inhibit a proper foreshock region. We predict that future missions, measuring the magnetosheath of Mercury, will find low numbers of jets due to low Alfvén Mach numbers.

Plain Language Summary

The Sun produces a constant outflow of particles and magnetic field, the solar wind. The Earth's magnetic field diverts that flow and protects us from these particles. A shock wave is built up between the magnetic field and the solar wind. Here, the particles get decelerated abruptly and form a turbulent region: the Earth's magnetosheath. Within the magnetosheath, we regularly find faster or denser flows of particles, which we call jets. How these jets get formed is part of active research. We look at times where the Sun bursts out huge particle clouds (coronal mass ejections, CMEs) in the direction of Earth and analyze, how these clouds affect the jet generation. We compare, how the conditions in the solar wind differ from the conditions in CMEs. Specifically, we look at values that affect the shock: the angle of the magnetic field and the Mach number. We then compare, how the conditions in the solar wind looks when jets get generated. We find that the CME decreases the generation of jets with its strong magnetic field and its rather randomly distributed magnetic field angle. With that, the CME change the properties of the bow shock and therefore the jet generation mechanisms.

1 Introduction

The magnetosheath is the region of shocked solar wind (SW) plasma sunward of the Earth's magnetosphere. First noticed by Němeček et al. (1998), the magnetosheath regularly shows dynamic pressure enhancements, which we shall call jets in the present work. Jets can show an increase in dynamic pressure up to 15 times compared to the surrounding plasma (Plaschke et al., 2013). Their median size is estimated to be 0.1 R_e but can reach up to more than 2 R_e (Plaschke et al., 2016, 2020). Large jets in particular can be geoeffective (Hietala et al., 2018; Nykyri et al., 2019; Norenius et al., 2021) and appear several times per hour (Plaschke et al., 2016).

Recently, several generation mechanisms were proposed to explain the occurrence of magnetosheath jets. We briefly describe those discussed in the literature, reviewed in Plaschke et al. (2018). Most mechanisms explain jets as a result of different processes in the foreshock region and are therefore associated with the quasi-parallel bow shock. The foreshock can only build up due to back-streaming ions from a super-critical bow shock and is therefore dependent on a high Alfvénic Mach number (Balogh & Treumann, 2013), which is defined as $M_A = v_{sw}/v_A$, with v_{sw} denoting the SW velocity, and $v_A = B/\sqrt{\mu_0 \rho}$ (with B being the magnetic field strength, μ_0 the magnetic permeability and ρ the SW density, respectively) defining the Alfvén velocity. The foreshock builds up sunward of the quasi-parallel shock front and therefore requires a low shock normal angle Θ_{Bn}. The interplanetary magnetic field (IMF) cone angle ($\arccos|B_x|/|B|$, with B_x denoting the magnetic field strength in GSE-X) is often used as a substitute for Θ_{Bn} for

the subsolar region (see e.g. Plaschke et al., 2013; Vuorinen et al., 2019; Raptis et al., 2020).

In general, results show that jets appear more often during low cone angle periods (Plaschke et al., 2013; Vuorinen et al., 2019; LaMoury et al., 2021). Phenomena in the foreshock can cause ripples in the bow shock (Balogh & Treumann, 2013). The way in which the SW is processed by the rippled shock has been proposed to be the cause for jet generation (Hietala et al., 2009; Hietala & Plaschke, 2013; Preisser et al., 2020). At the ripple, the local oblique shock front may cause the deceleration of the incoming SW plasma to be less efficient in the GSE-X direction in comparison to the less oblique shock surroundings. It would create a flow (jet) in the downstream side of the shock that is faster than the surrounding shocked and decelerated plasma. This rippling effect as well as the integration of fast foreshock flows into the magnetosheath might also be a consequence of short large-amplitude magnetic field structures (SLAMS) forming in the foreshock (Schwartz & Burgess, 1991; Karlsson et al., 2015). The latest simulations have shown that the majority of jets can be related to foreshock compressional structures (Suni et al., 2021). Recently, Raptis et al. (2022) presented evidence that jets can be generated as a consequence of the bow shock reformation process at the quasi-parallel shock front itself. This has been also proposed to be a mechanism for the formation of paramagnetic embedded plasmoids based on hybrid simulations (Preisser et al., 2020). Hietala and Plaschke (2013) estimated that the majority of jets can be associated to bow shock rippling. A subset of jets can be explained by other mechanisms. For example, Archer et al. (2012) suggested that rotational discontinuities in the magnetic field cause pressure pulses in the magnetosheath every time we see a change form the quasi-parallel to the quasi-perpendicular shock region and vice-versa.

In a recent statistical study Koller et al. (2022) analyzed jet occurrence within large scale SW structures, such as transient coronal mass ejections (CMEs) and stream interaction regions (SIRs) together with their high speed streams (HSSs). It was found that jets are less frequent when the magnetic ejecta (ME) region of the CME passes Earth. In comparison to quiet SW conditions and compressed SW for SIRs, CMEs and their ME regions present "laboratories" with very different SW conditions. Typically, CMEs are faster than the SW and can drive shocks which generate two separate density structures: compressed and piled up SW in the sheath and leading edge (see Temmer & Bothmer, 2022), followed by a strong and smoothly rotating magnetic flux rope. Fig. 1 shows a CME example measured by the Active Composition Explorer (ACE, Stone et al., 1998). In the present work, we therefore investigate on the basis of these recent results the physical mechanism of the decrease in jet occurrence and suppression of jets. The results will give us a better understanding of jet production mechanisms. We hypothesize that the conditions inside the CME-ME pose difficulties for the building of a proper foreshock. Due to the twisted magnetic field lines in the flux rope inside of the ME, the IMF cone angle could differ greatly from radial IMF conditions. Radial IMF lines however seem to be a necessary condition to generate a quasi-parallel shock region that builds the foreshock. In addition to that, the high magnetic field strength and low density inside a CME-ME cause an increase in Alfvén velocity. Thus, the Alfvén Mach number decreases, causing a decrease in the strength of the bow shock. The sum of all these effects generated by the arrival of the CME-ME to the bow shock could inhibit the building of a foreshock region that can efficiently generate jets near the subsolar point.

To test our hypothesis, we look at jets detected by THEMIS spacecraft between 2008 and 2021 and compare the SW conditions during these times.

2 Data

We compare in situ SW plasma and magnetic field data from OMNI during times when jets are observed with the SW measured during CMEs and as a reference during

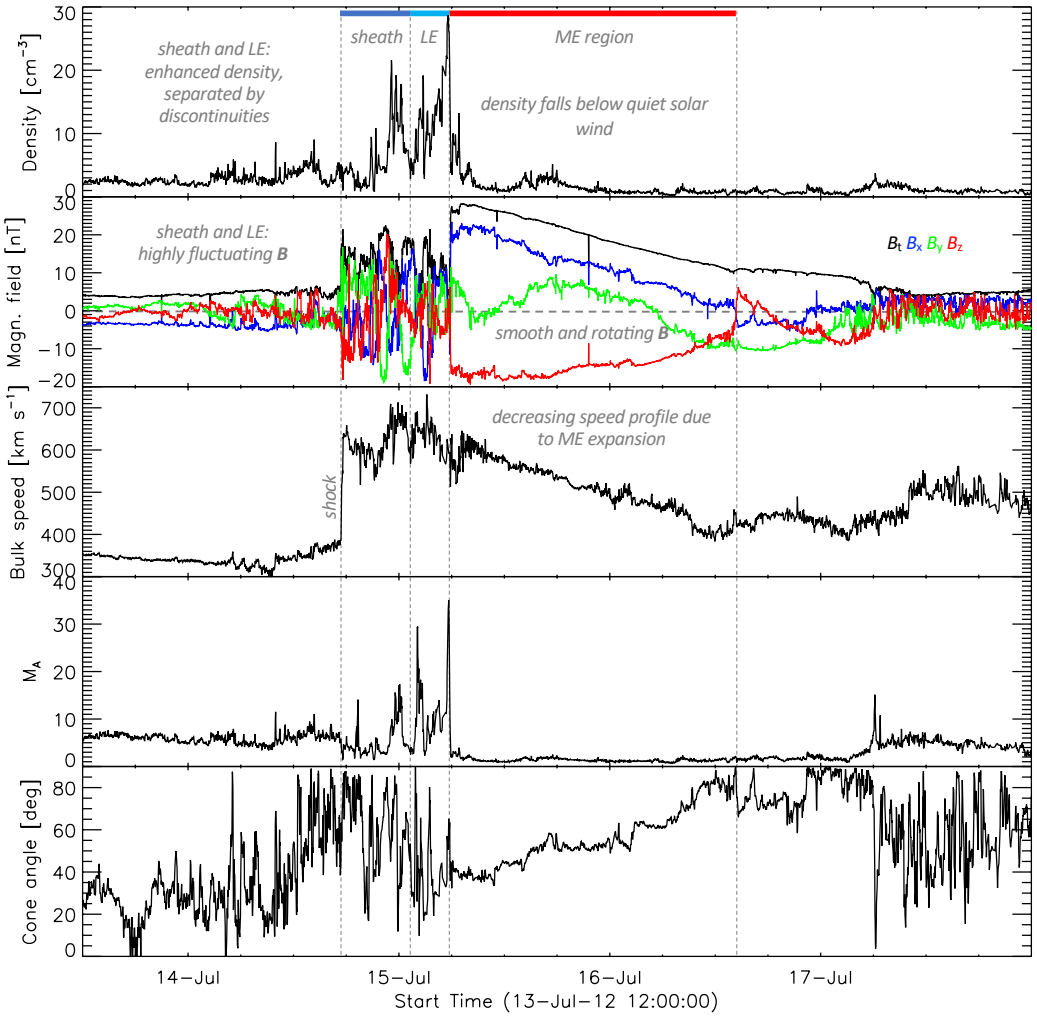

Figure 1. Example of a CME from ACE measurements. The three panels from top to bottom show the measured proton density, total magnetic field and vector components in GSE coordinates (see legend), and the proton bulk speed. This CME clearly reveals the typical structures, shock, two density enhancements — sheath (dark blue) and leading edge (LE, light blue) — followed by the ME with the twisted field components. The next two panels give the calculated Alfvénic Mach number and the cone angle (see more details in the text).

all times when magnetosheath data were available. We use 1-min resolution OMNI velocity, magnetic field, and density data (King & Papitashvili, 2005). Our data covers the time range between January 2008 and December 2021.

Data from the THEMIS spacecraft (Angelopoulos, 2008) are used to detect intervals of jets in the magnetosheath. Specifically, we use the reduced ion moments from the (ion velocity, density, temperature, and energy flux) from the THEMIS Electrostatic Analyzer (ESA McFadden et al., 2008). We use magnetic field measurements from the Fluxgate Magnetometer (FGM Auster et al., 2008).

Magnetosheath intervals are determined by the same criteria used in Plaschke et al. (2013) and Koller et al. (2022): The spacecraft GSE position is restricted to 7–18 R_e and has to be within a 30° Sun-centered cone with tip at the Earth. To ensure that the spacecraft is within the magnetosheath, the ion density has to be at least twice as dense as the upstream solar wind. The energy flux of the 10 keV ions has to be less than those of the 1 keV ions. The magnetosheath intervals are required to be longer than 2 min.

Jets were defined using the criteria of Archer and Horbury (2013): $p_{\mathrm{dyn}} > 2 \times \langle p_{\mathrm{dyn}} \rangle_{20\mathrm{min}}$. Here, $\langle p_{\mathrm{dyn}} \rangle_{20\mathrm{min}}$ denotes the 20 minute running average of the magnetosheath dynamic pressure. Therefore, enhancements of the dynamic pressure larger than two times of the surrounding plasma within 20 minutes are declared as jets. Magnetosheath intervals shorter than 20 minutes are not considered for jet detection. Jets were restricted to only those with a duration of more than 5 seconds. Using these criteria, we detected a total 51737 jets within the given time range. The intervals of magnetosheath and jet times are provided at `https://osf.io/hwkum/` as given in Koller et al. (2022).

Arrival times of ICMEs at Earth are collected in an online catalogue maintained by Richardson and Cane (Cane & Richardson, 2003; Richardson & Cane, 2010). It includes a variety of information on near-Earth CMEs that have been detected since 1996. We use the start and end times of CME-MEs (labeled as ICME Plasma/Field Start, End) in our work, which are the times that were measured by ACE.

3 Analysis

We calculate mean OMNI values during jet intervals and during all times when we have simultaneously magnetosheath observations by THEMIS. The latter is used as a reference to determine, how the SW parameters are distributed during jet detection times. For each time interval, we calculate the mean SW Alfvénic Mach number and the IMF cone angle. One mean Mach number and cone angle value was determined for each jet. The SW reference conditions datapoints have a 1-min resolution. To check how important these parameter are for the jet production, we plot a 2-dimensional (2D) histogram with the cone angle on the x-axis and the Mach number on the y-axis. All histograms are normalized to the peak value. Bin sizes of 4.8 ° for the x-axis and 1.6 for the y-axis were chosen. These bin sizes ensure reliable amounts of data as well as reasonable resolution for our analysis.

We then determine the jet probability distribution as a function of Alfvén Mach number and IMF cone angle. We do this by dividing the SW conditions that we find during jets by the overall SW conditions. This results in a 2D histogram plot, where the jet probability is color-coded in each bin. As a final analysis we check, how this jet probability distribution compares to the SW conditions that we find within CME-MEs.

4 Results

The left plot of Fig.2 shows the 2D histogram distribution for the SW condition during all times when we have magnetosheath observations. The SW condition peak at cone angles of 40–90 ° and Mach numbers around 6–12. This distribution serves as a ref-

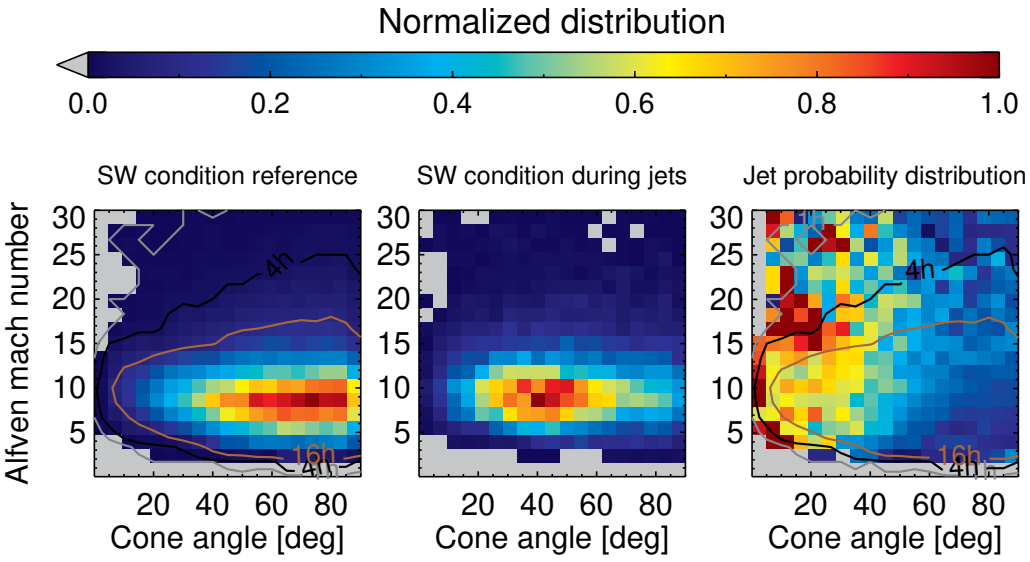

Figure 2. 2D histogram showing normalized distributions of cone angle and Mach number. The left plot shows the overall distribution of both parameter in the SW during all observation times. The middle plot shows the SW parameter distribution during jet detection. The right plot shows the jet probability depending of both parameters. Contours indicate, how many hours of data we have for each bin. Most reliable data are marked by the 16 h contour (in brown).

erence for the further analysis. The distribution of SW conditions during jets is shown in the middle plot of Fig. 2. We find that jets appear dominantly during cone angles of 20–50 and Mach numbers of 6–11.

The right plot of Fig. 2 shows the normalized jet probability. Here, the distribution of SW condition during jets is divided by the reference SW distribution. Contours on this figure show the amount of available magnetosheath observation time per bin. It represents the data from the reference values. The innermost contour (in brown) indicates that within this area, each bin in the 2D plot consists of 16 h or more of magnetosheath observation time, making these areas the most reliable to our analysis. As expected, the jets are found predominantly at lower cone angles, mostly at values lower than 40 °. Jets are rarely detected during intervals with high cone angles. The jet probability during high cone angles (> 50 °) decreases for low Mach numbers (< 5). During these conditions, the probability to detect jets is roughly six to seven times lower compared to times of low cone angle (< 40 °) and high Mach numbers (> 5). This value is similar to the probability of detecting jets downstream of the quasi-parallel shock compared to the quasi-perpendicular shock found by Archer and Horbury (2013). The right plot of Fig.2 also shows that the jet probability at low mach numbers (< 5) is significantly decreasing even for intermediate cone angles (30–50 °).

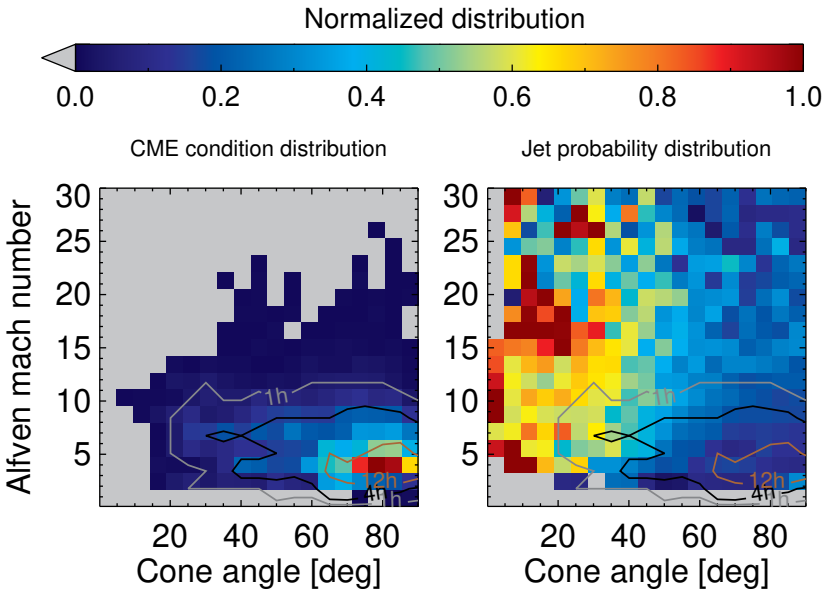

Figure 3. 2D histogram showing normalized distributions of cone angle and Mach number. The left plot shows the overall distribution of both parameter in the SW during CME-MEs. The right plot shows again the overall jet probability distribution (rightmost plot in Fig. 2), overplotted with contours of data availability during CME-MEs.

The mean SW conditions that we can find during CME-MEs is shown in the left plot of Fig. 3. The same bin sizes from the previous plot (4.8 ° for the x-axis and 1.6 for the y axis) were chosen. The distribution is confined mostly to the area at cone angle higher than 60 ° and Mach numbers between 2 and 5.

The right plot of Fig. 3 is the same as the right plot of Fig. 2, showing the jet probability distribution, however, overlaid with the contours for the mean SW conditions found during CME-MEs using the values taken from the left plot of Fig. 3. The innermost contour (in brown) reveals CME-ME bins with data availabilities of more than 12 h. Again, the distribution is confined mostly to the area at the lower right corner of the 2D-histogram plot. The SW conditions during CMEs overlay the area where we find the lowest probability of detecting jets.

5 Discussion and Conclusion

For the first time, we analyze how the distinct conditions within CME-MEs influence the parameters necessary to produce jets efficiently. We suggest that the high IMF cone angle found in the CME-MEs renders the building of a foreshock difficult. In addition to this, sufficiently weak Mach numbers might hinder the backstreaming of ions and thus the building of the foreshock and the reformation of the quasi-parallel shock.

Our findings are further supported by simulation results done by Tinoco-Arenas et al. (2022). The appearance of jets ceased at shocks with very low Alfvén Mach numbers. Similarly, high Θ_{Bn} angles (here as a proxy we use the cone angle at the subsolar point) caused a reduction of jet production in their simulations.

While the number of detected jets is significantly lower within CMEs (Koller et al., 2022), there is still a non-vanishing amount of them. Whether these jets are different compared to jets during low- cone angle and high-Alfvénic conditions will give insight in their generation mechanisms. The overall probability distribution of jets that were only detected during CME-MEs (not shown) follows the same probability distribution as shown in the right plot of Fig. 2. The only significant difference being that the favorable conditions for the jet generation are rarer within CME-MEs.

With Θ_{Bn} (and as proxy the cone angle) having the most influence on the jet production, there is the question whether the foreshock builds up at positions far away from the Earth-Sun line (as sketched in Fig. 1 by Vuorinen et al., 2019).

At the planet Mercury, we also find low Alfvénic Mach numbers similar to what we find within CME-MEs at 1 AU. Karlsson et al. (2016) analyzed isolated magnetic field structures within the Hermean magnetosheath (Anderson et al., 2010) as possible analogues to terrestrial jets. However, the analyzed structures had no dependence on the Θ_{Bn} distribution, making the connection to the classical magnetosheath jets detected at Earth uncertain. Sundberg et al. (2015) suggested that the low mach number might not lead to a proper foreshock. This could be similar to what we see at the Earth's bow shock during CME-MEs. Based on our result, we postulate that the number of jets within the Hermean magnetosheath would be low. The BepiColombo mission will insert into an orbit around Mercury between December 2025 and March 2026 (Milillo et al., 2020). This mission will give new insights on the jet occurrence and generation at the Hermean magnetosheath and foreshock.

In summary, we show that a mix of high cone angles and low Mach numbers are unfavorable SW conditions, hence, decreasing the production of jets in the magnetosheath. The condition within CME-MEs is similar to this condition, which gives context to the low detection number of jets in this structure as was reported by Koller et al. (2022). Without a proper foreshock, the proposed jet generation mechanisms for the majority of jets is not applicable. Further investigation into the exact details is necessary to conclude, how the CME is disrupting the foreshock. Future case studies as well as simulations on the interaction of CMEs with the bow shock can complement our statistical work. A next step is to analyze, whether the jets found during different structures have statistically distinctive differences in their properties.

Data Availability Statement

We thank C. W. Carlson and J. P. McFadden for use of ESA data. We acknowledge the use of NASA/ GSFC's Space Physics Data Facility's OMNI data and web services (`https://omniweb.gsfc.nasa.gov/html/omni_min_data.html`). THEMIS and OMNI data were accessed using the SPEDAS software (Angelopoulos et al., 2019). We provide the jet lists as well as the magnetosheath times at `https://osf.io/hwkum/`.

Acknowledgments

F.K., M.T., L.P., O.R., and F.P. gratefully acknowledge the Austrian Science Fund (FWF): P 33285-N for supporting this project. We acknowledge NASA contract NAS5-02099 and V. Angelopoulos for use of data from the THEMIS Mission. Specifically we thank K.H. Glassmeier, H.U. Auster and W. Baumjohann for the use of FGM data provided under the lead of the Technical University of Braunschweig and with financial support through the German Ministry for Economy and Technology and the German Center for Aviation and Space (DLR) under contract 50 OC 0302.

References

Anderson, B. J., Acuña, M. H., Korth, H., Slavin, J. A., Uno, H., Johnson, C. L., ... McNutt, R. L. (2010, May). The Magnetic Field of Mercury. *Space Science Reviews*, *152*(1-4), 307-339. doi: 10.1007/s11214-009-9544-3

Angelopoulos, V. (2008, December). The THEMIS Mission. *Space Science Reviews*, *141*(1-4), 5-34. doi: 10.1007/s11214-008-9336-1

Archer, M. O., & Horbury, T. S. (2013, February). Magnetosheath dynamic pressure enhancements: occurrence and typical properties. *Annales Geophysicae*, *31*(2), 319-331. doi: 10.5194/angeo-31-319-2013

Archer, M. O., Horbury, T. S., & Eastwood, J. P. (2012, May). Magnetosheath pressure pulses: Generation downstream of the bow shock from solar wind discontinuities. *Journal of Geophysical Research (Space Physics)*, *117*(A5), A05228. doi: 10.1029/2011JA017468

Auster, H. U., Glassmeier, K. H., Magnes, W., Aydogar, O., Baumjohann, W., Constantinescu, D., ... Wiedemann, M. (2008, December). The THEMIS Fluxgate Magnetometer. *Space Science Reviews*, *141*(1-4), 235-264. doi: 10.1007/s11214-008-9365-9

Balogh, A., & Treumann, R. A. (2013). *Physics of Collisionless Shocks* (Vol. 12). doi: 10.1007/978-1-4614-6099-2

Cane, H. V., & Richardson, I. G. (2003, April). Interplanetary coronal mass ejections in the near-Earth solar wind during 1996-2002. *Journal of Geophysical Research (Space Physics)*, *108*(A4), 1156. doi: 10.1029/2002JA009817

Hietala, H., Laitinen, T. V., Andréeová, K., Vainio, R., Vaivads, A., Palmroth, M., ... Rème, H. (2009, December). Supermagnetosonic Jets behind a Collisionless Quasiparallel Shock. *Physical Review Letters*, *103*(24), 245001. doi: 10.1103/PhysRevLett.103.245001

Hietala, H., Phan, T. D., Angelopoulos, V., Oieroset, M., Archer, M. O., Karlsson, T., & Plaschke, F. (2018, February). In Situ Observations of a Magnetosheath High-Speed Jet Triggering Magnetopause Reconnection. *Geophysics Research Letters*, *45*(4), 1732-1740. doi: 10.1002/2017GL076525

Hietala, H., & Plaschke, F. (2013, November). On the generation of magnetosheath high−speed jets by bow shock ripples. *Journal of Geophysical Research (Space Physics)*, *118*(11), 7237-7245. doi: 10.1002/2013JA019172

Karlsson, T., Kullen, A., Liljeblad, E., Brenning, N., Nilsson, H., Gunell, H., & Hamrin, M. (2015, September). On the origin of magnetosheath plasmoids and their relation to magnetosheath jets. *Journal of Geophysical Research (Space Physics)*, *120*(9), 7390-7403. doi: 10.1002/2015JA021487

Karlsson, T., Liljeblad, E., Kullen, A., Raines, J. M., Slavin, J. A., & Sundberg, T. (2016, September). Isolated magnetic field structures in Mercury's magnetosheath as possible analogues for terrestrial magnetosheath plasmoids and jets. *Planetary and Space Science*, *129*, 61-73. doi: 10.1016/j.pss.2016.06.002

King, J. H., & Papitashvili, N. E. (2005, February). Solar wind spatial scales in and comparisons of hourly Wind and ACE plasma and magnetic field data. *Journal of Geophysical Research (Space Physics)*, *110*(A2), A02104. doi: 10.1029/2004JA010649

Koller, F., Plaschke, F., Temmer, M., Preisser, L., Roberts, O. W., Weiss, S., & Vörös, Z. (2022, Jul). *Themis local magnetosheath jet data 2008-2021.* OSF. Retrieved from `osf.io/hwkum`

Koller, F., Temmer, M., Preisser, L., Plaschke, F., Geyer, P., Jian, L. K., ... LaMoury, A. T. (2022). Magnetosheath jet occurrence rate in relation to cmes and sirs. *Journal of Geophysical Research: Space Physics*, *127*(4), e2021JA030124. Retrieved from `https://agupubs.onlinelibrary.wiley.com/doi/abs/10.1029/2021JA030124` (e2021JA030124 2021JA030124) doi: https://doi.org/10.1029/2021JA030124

LaMoury, A. T., Hietala, H., Plaschke, F., Vuorinen, L., & Eastwood, J. P. (2021).

Solar wind control of magnetosheath jet formation and propagation to the magnetopause. *Journal of Geophysical Research: Space Physics*, *126*(9), e2021JA029592. Retrieved from `https://agupubs.onlinelibrary.wiley.com/doi/abs/10.1029/2021JA029592` (e2021JA029592 2021JA029592) doi: https://doi.org/10.1029/2021JA029592

McFadden, J. P., Carlson, C. W., Larson, D., Ludlam, M., Abiad, R., Elliott, B., ... Angelopoulos, V. (2008, December). The THEMIS ESA Plasma Instrument and In-flight Calibration. *Space Science Reviews*, *141*(1-4), 277-302. doi: 10.1007/s11214-008-9440-2

Milillo, A., Fujimoto, M., Murakami, G., Benkhoff, J., Zender, J., Aizawa, S., ... Wahlund, J. E. (2020, July). Investigating Mercury's Environment with the Two-Spacecraft BepiColombo Mission. *Space Science Reviews*, *216*(5), 93. doi: 10.1007/s11214-020-00712-8

Norenius, L., Hamrin, M., Goncharov, O., Gunell, H., Opgenoorth, H., Pitkänen, T., ... Baddeley, L. (2021, August). Ground-Based Magnetometer Response to Impacting Magnetosheath Jets. *Journal of Geophysical Research (Space Physics)*, *126*(8), e29115. doi: 10.1029/2021JA029115

Němeček, Z., Šafránková, J., Přech, L., Sibeck, D. G., Kokubun, S., & Mukai, T. (1998, January). Transient flux enhancements in the magnetosheath. *Geophysics Research Letters*, *25*(8), 1273-1276. doi: 10.1029/98GL50873

Nykyri, K., Bengtson, M., Angelopoulos, V., Nishimura, Y., & Wing, S. (2019, June). Can Enhanced Flux Loading by High-Speed Jets Lead to a Substorm? Multipoint Detection of the Christmas Day Substorm Onset at 08:17 UT, 2015. *Journal of Geophysical Research (Space Physics)*, *124*(6), 4314-4340. doi: 10.1029/2018JA026357

Plaschke, F., Hietala, H., & Angelopoulos, V. (2013, October). Anti-sunward high-speed jets in the subsolar magnetosheath. *Annales Geophysicae*, *31*(10), 1877-1889. doi: 10.5194/angeo-31-1877-2013

Plaschke, F., Hietala, H., Angelopoulos, V., & Nakamura, R. (2016, April). Geoeffective jets impacting the magnetopause are very common. *Journal of Geophysical Research (Space Physics)*, *121*(4), 3240-3253. doi: 10.1002/2016JA022534

Plaschke, F., Hietala, H., Archer, M., Blanco-Cano, X., Kajdič, P., Karlsson, T., ... Sibeck, D. (2018, August). Jets Downstream of Collisionless Shocks. *Space Science Reviews*, *214*(5), 81. doi: 10.1007/s11214-018-0516-3

Plaschke, F., Hietala, H., & Vörös, Z. (2020, September). Scale Sizes of Magnetosheath Jets. *Journal of Geophysical Research (Space Physics)*, *125*(9), e27962. doi: 10.1029/2020JA027962

Preisser, L., Blanco-Cano, X., Kajdič, P., Burgess, D., & Trotta, D. (2020, September). Magnetosheath Jets and Plasmoids: Characteristics and Formation Mechanisms from Hybrid Simulations. *The Astrophysical Journal Letters*, *900*(1), L6. doi: 10.3847/2041-8213/abad2b

Raptis, S., Karlsson, T., Plaschke, F., Kullen, A., & Lindqvist, P.-A. (2020, November). Classifying Magnetosheath Jets Using MMS: Statistical Properties. *Journal of Geophysical Research (Space Physics)*, *125*(11), e27754. doi: 10.1029/2019JA027754

Raptis, S., Karlsson, T., Vaivads, A., Pollock, C., Plaschke, F., Johlander, A., ... Lindqvist, P.-A. (2022, December). Downstream high-speed plasma jet generation as a direct consequence of shock reformation. *Nature Communications*, *13*(1), 598. Retrieved 2022-03-13, from `https://www.nature.com/articles/s41467-022-28110-4` doi: 10.1038/s41467-022-28110-4

Richardson, I. G., & Cane, H. V. (2010, June). Near-Earth Interplanetary Coronal Mass Ejections During Solar Cycle 23 (1996 - 2009): Catalog and Summary of Properties. *Solar Physics*, *264*(1), 189-237. doi: 10.1007/s11207-010-9568-6

Schwartz, S. J., & Burgess, D. (1991, March). Quasi-parallel shocks: A patchwork of three-dimensional structures. *Geophysical Research Letters*, *18*(3), 373-376.

360 doi: 10.1029/91GL00138
361 Stone, E. C., Frandsen, A. M., Mewaldt, R. A., Christian, E. R., Margolies, D.,
362 Ormes, J. F., & Snow, F. (1998, July). The Advanced Composition Explorer.
363 *Space Science Reviews*, *86*, 1-22. doi: 10.1023/A:1005082526237
364 Sundberg, T., Boardsen, S. A., Burgess, D., & Slavin, J. A. (2015, September). Co-
365 herent wave activity in Mercury's magnetosheath. *Journal of Geophysical Re-*
366 *search (Space Physics)*, *120*(9), 7342-7356. doi: 10.1002/2015JA021499
367 Suni, J., Palmroth, M., Turc, L., Battarbee, M., Johlander, A., Tarvus, V., ...
368 Zhou, H. (2021, October). Connection Between Foreshock Structures and the
369 Generation of Magnetosheath Jets: Vlasiator Results. *Geophysical Research*
370 *Letters*, *48*(20), e95655. doi: 10.1029/2021GL095655
371 Temmer, M., & Bothmer, V. (2022, February). Characteristics and evolution of
372 sheath and leading edge structures of interplanetary coronal mass ejections in
373 the inner heliosphere based on Helios and Parker Solar Probe observations.
374 *arXiv e-prints*, arXiv:2202.04391.
375 Tinoco-Arenas, A., Kajdič, P., Preisser, L., Blanco-Cano, X., Trotta, D., & Burgess,
376 D. (2022, February). Parametric study of magnetosheath jets in 2D local
377 hybrid simulations. *Frontiers in Astronomy and Space Sciences*, *9*, 5. doi:
378 10.3389/fspas.2022.793195
379 Vuorinen, L., Hietala, H., & Plaschke, F. (2019, August). Jets in the magnetosheath:
380 IMF control of where they occur. *Annales Geophysicae*, *37*(4), 689-697. doi: 10
381 .5194/angeo-37-689-2019